Nonlinear and Linear Evolution of Initial Forecast Errors

TOMISLAVA VUKICEVIC

National Center for Atmospheric Research, Boulder, Colorado

(Manuscript received 8 August 1990, in final form 10 January 1991)

ABSTRACT

The hypothesis that the short-time evolution of forecast errors originating from initial data uncertainties can be approximated by linear model solutions is investigated using a realistic prognostic model. A tangent linear limited-area model based on a state of the art mesoscale numerical forecast model is developed. The linearization is performed with respect to a temporally and spatially varying basic state. The basic state fields are produced by the nonlinear model using observed data.

The tangent model solutions and the error fields based on the nonlinear integrations are compared. The results demonstrate that the initial error evolution is well represented by the tangent model for periods of 1–1.5 days duration. The linear model solutions based on the time-independent basic state are also good approximations of the real-error evolutions, providing the prognostic fields are not changing rapidly in time.

The application of the linear model for estimating appropriate initial perturbation for the initial error sensitivity study is illustrated using a simple method. Comparison between the nonlinear integrations based on the unstable initial perturbation and an arbitrarily selected initial perturbation shows that the latter initialization can produce misleading results.

1. Introduction

It is well known that the errors originating from initial data uncertainties grow in numerical forecasts. Global numerical models explicitly treat only processes with characteristic horizontal scales longer than several hundred kilometers. Consequently, the error growth occurring in these models is associated with synoptic scale dynamics. In a recent paper Vukicevic and Errico (1990; hereafter referred to as VE) have shown that even for high-resolution limited-area model forecasts the initial error growth is confined to the synoptic scales.

This suggests that the initial error growth in numerical forecasts is associated with synoptic-scale flow barotropic and baroclinic instabilities (e.g., Lorenz 1969; Thompson 1957; Lacarra and Talagrand 1988; Kallen and Huang 1988). These instabilities are typically studied using a linear dynamics framework. The same framework can be applied to studying the initial forecast error evolution. This approach was used in the Lacarra and Talagrand's (1988) study based on the shallow-water f-plane model. They have shown that the short-time evolution of the initial errors for this model was well represented by the linear tangent differential model solutions. They have also demonstrated that the solutions based on the time-independent linear model coefficients were very similar to the tangent model solutions. Lacarra and Talagrand have suggested application of their results to data assimilation procedures that require short-time error evolution estimates.

In this study we investigate linearity of initial error evolution using a state of the art primitive equation limited-area model. Such a sophisticated limited area model is typically used for short- to medium-range predictions based on observed data. Therefore, the tangent model experiments performed for such a model would rigorously test the hypothesis of the linearity of error evolution in numerical forecasts and may be very useful for upper-bound initial forecast error estimates and for data assimilation purposes.

The method used for the linearity test and the nonlinear and linear numerical models used for the numerical experiments are described in section 2. The short-time error evolution based on the nonlinear and linear integrations is shown in section 3. The application of the linear model and the unstable linear solutions are discussed in section 4. A brief summary and conclusions are presented in section 5.

2. Method and models

The method used in this study is simple. First, the linear version of a sophisticated nonlinear numerical forecast model is developed. The linearization and the numerical linear model are described in this section. Then, the forecast errors originating from the initial data errors are evaluated from the nonlinear and linear numerical solutions and compared.

Corresponding author address: Dr. Tomislava Vukicevic, NCAR, P.O. Box 3000, Boulder, CO 80303.

The nonlinear numerical model used in this study is the mesoscale model developed jointly at the Pennsylvania State University and the National Center for Atmospheric Research, designated MM4 (Anthes et al. 1987). The specific version of this model used for the nonlinear numerical experiments described in this study and the initial forecast error evolution associated with this version of the MM4 are described in detail in VE.

For the linear model integrations the error fields produced by the nonlinear integrations at selected forecast time are used as the initial conditions. The basic state fields for the linear model are also provided by the nonlinear model integrations.

Linear model. The MM4 is based on the set of primitive equations written in flux form. We have linearized these equations with respect to a spatially and temporally varying basic state. Since the basic state is allowed to have temporal variation, the resulting linear system of equations is the tangent linear system. The tangent, therefore, is defined with respect to the nonlinear model solution trajectories in phase space. The tangent linear model based on the MM4 set of equations is given by

$$\frac{\partial(\bar{p}^*u)}{\partial t} = -m^2\left[\frac{\partial}{\partial x}\left(\frac{\bar{p}^*\bar{u}u}{m}\right) + \frac{\partial}{\partial y}\left(\frac{\bar{p}^*\bar{v}u}{m}\right)\right] - \frac{\partial}{\partial\sigma}(\bar{p}^*u\dot{\bar{\sigma}}) - m\bar{p}^*\left[\frac{R\bar{T}}{(\bar{p}^* + p_t/\sigma)}\frac{\partial p^*}{\partial x} + \frac{\partial\phi}{\partial x}\right] + f\bar{p}^*v + F_U - m^2\left(\frac{\bar{p}^*u}{m}\frac{\partial\bar{u}}{\partial x} + \frac{\bar{p}^*v}{m}\frac{\partial\bar{u}}{\partial y}\right) - \dot{\sigma}\bar{p}^*\frac{\partial\bar{u}}{\partial\sigma} + m\bar{p}^*\frac{R}{(\bar{p}^* + p_t/\sigma)} \times \frac{\bar{T}p^* - T(\bar{p}^* + p_t/\sigma)}{(\bar{p}^* + p_t/\sigma)}\frac{\partial\bar{p}^*}{\partial x} \quad (1a)$$

$$\frac{\partial(\bar{p}^*v)}{\partial t} = -m^2\left[\frac{\partial}{\partial x}\left(\frac{\bar{p}^*\bar{u}v}{m}\right) + \frac{\partial}{\partial y}\left(\frac{\bar{p}^*\bar{v}v}{m}\right)\right] - \frac{\partial}{\partial\sigma}(\bar{p}^*v\dot{\bar{\sigma}}) - m\bar{p}^*\left[\frac{R\bar{T}}{(\bar{p}^* + p_t/\sigma)}\frac{\partial p^*}{\partial y} + \frac{\partial\phi}{\partial y}\right] - f\bar{p}^*u + F_V - m^2\left(\frac{\bar{p}^*u}{m}\frac{\partial\bar{v}}{\partial x} + \frac{\bar{p}^*v}{m}\frac{\partial\bar{v}}{\partial y}\right) - \dot{\sigma}\bar{p}^*\frac{\partial\bar{v}}{\partial\sigma} + m\bar{p}^*\frac{R}{(\bar{p}^* + p_t/\sigma)} \times \frac{\bar{T}p^* - T(\bar{p}^* + p_t/\sigma)}{(\bar{p}^* + p_t/\sigma)}\frac{\partial\bar{p}^*}{\partial y} \quad (1b)$$

$$\frac{\partial(\bar{p}^*T)}{\partial t} = -m^2\left[\frac{\partial}{\partial x}\left(\frac{\bar{p}^*\bar{u}T}{m}\right) + \frac{\partial}{\partial y}\left(\frac{\bar{p}^*\bar{v}T}{m}\right)\right] - \frac{\partial}{\partial\sigma}(\bar{p}^*T\dot{\bar{\sigma}}) + \frac{R\bar{p}^*(T\bar{\omega} + \bar{T}\omega)}{c_p(\sigma\bar{p}^* + p_t)} + F_T - m^2\left(\frac{\bar{p}^*u}{m}\frac{\partial\bar{T}}{\partial x} + \frac{\bar{p}^*v}{m}\frac{\partial\bar{T}}{\partial y}\right) - \dot{\sigma}\bar{p}^*\frac{\partial\bar{T}}{\partial\sigma} - \frac{R\bar{T}\bar{\omega}\sigma\bar{p}^*p^*}{c_p(\sigma\bar{p}^* + p_t)^2} \quad (1c)$$

$$\frac{\partial p^*}{\partial t} = -m^2\int_0^1\left[\frac{\partial}{\partial x}\left(\frac{\bar{p}^*u}{m}\right) + \frac{\partial}{\partial y}\left(\frac{\bar{p}^*v}{\partial m}\right) + \frac{\partial}{\partial x}\left(\frac{p^*\bar{u}}{m}\right) + \frac{\partial}{\partial y}\left(\frac{p^*\bar{v}}{m}\right)\right]d\sigma \quad (1d)$$

$$\dot{\sigma} = -\frac{1}{\bar{p}^*}\int_0^\sigma\left\{\frac{\partial p^*}{\partial t} + m^2\left[\frac{\partial}{\partial x}\left(\frac{\bar{p}^*u}{m}\right) + \frac{\partial}{\partial y}\left(\frac{\bar{p}^*v}{m}\right) + \frac{\partial}{\partial x}\left(\frac{p^*\bar{u}}{m}\right) + \frac{\partial}{\partial y}\left(\frac{p^*\bar{v}}{m}\right)\right]\right\}d\sigma - \frac{p^*}{\bar{p}^*}\dot{\bar{\sigma}} \quad (1e)$$

$$\omega = p^*\dot{\bar{\sigma}} + \bar{p}^*\dot{\sigma} + \sigma\frac{dp^*}{dt} \quad (1f)$$

and

$$\frac{dp^*}{dt} = \frac{\partial p^*}{\partial t} + m\left(\bar{u}\frac{\partial p^*}{\partial x} + \bar{v}\frac{\partial p^*}{\partial y} + u\frac{\partial\bar{p}^*}{\partial x} + v\frac{\partial\bar{p}^*}{\partial y}\right)$$

$$\frac{\partial\phi}{\partial\ln(\sigma + p_t/\bar{p}^*)} = -RT \quad (1g)$$

where x, y, σ, and t are zonal, meridional, vertical, and time coordinates, respectively. The prognostic variables u, v, T, and $p^* = (p_s - p_t)$ are perturbations of the zonal and meridional wind components, temperature, and the surface pressure minus the model top-level pressure, respectively. The diagnostic variables in (1a)–(1g) are the geopotential ϕ, sigma coordinate vertical velocity $\dot{\sigma}$, and the pressure coordinate vertical velocity ω. Standard notation is used for the Coriolis coefficient f, the gas constant R, and the specific heat for dry air at constant pressure c_p. The barred variables in (1a)–(1g) represent the basic-state variables. All diabatic processes are neglected in the linear model with the exception of diffusion. The linear diffusion is represented by the F_U, F_V, and F_T terms in (1a)–(1c).

The numerical model based on (1a)–(1g), designated LMM4, was developed using the same finite difference schemes used in the nonlinear MM4. The gridpoint values for the basic-state variables were provided by the MM4 forecast. The linear model takes less computational time than the nonlinear model because most of the subgrid-scale parameterizations are excluded from the linear model.

3. Short-time error evolution

a. Nonlinear integrations

The numerical experiments based on the nonlinear version of the model were performed in the same manner as in VE. The MM4 was applied to large horizontal domains (approximately 9000 × 6400 km^2, longitude × latitude) using a horizontal resolution of 120 km

and 10 sigma levels in the vertical domain. The large horizontal domains were used in order to avoid the constraining effect of lateral boundary conditions upon the error evolution (Vukicevic and Paegle 1989). Vukicevic and Errico (1990) have shown that the initial errors grow in the MM4 integrations only if the integration domain is sufficiently large to allow free evolution of the error-field synoptic scales.

Since we are interested in the application of the linear model to different flow regimes, we use three distinctly different observed synoptic cases for our numerical experiments. These are: 1) the Alpine lee cyclogenesis observed during the 0000 UTC 5 March 1982–1200 UTC 6 March 1982 period, 2) the low-level jet occurrence southeast of the Alps in Europe observed during the 1200 UTC 23 March 1982–0000 UTC 25 March 1982 period, and 3) the explosive cyclogenesis over the western Atlantic observed during the 1200 UTC 13 February 1982–0000 UTC 15 February 1982 period. For brevity these cases are hereafter referred to as LECY (leecyclogenesis), LLJE (low-level jet), and EXCY (explosive cyclogenesis). The observed synoptic situation, forecast, and initial forecast error evolution for the LECY and LLJE cases are described in detail in VE. The observed evolution of the EXCY case and the MM4 forecast for this case are discussed in Kuo and Low-Nam (1990). The initial error sensitivity experiment for the EXCY case is performed in this study using the same experiment design as for the LECY and LLJE cases described in VE, but only one initial perturbation is considered in the present study, unlike in VE where the ensemble of initial perturbations is used.

The summary of the nonlinear results is as follows

1) the initial errors grow in the LECY and LLJE experiments and decay in the EXCY experiment. We would like to point out that the latter result is based on a single perturbation experiment.

2) The error growth rate is larger for the LECY case than for the LLJE case.

3) For all cases, the error fields have predominantly synoptic-scale features in the horizontal domain and large-scale features in the vertical domain after only 12 h of integration. It is important to note that these error fields originate from the initial error fields that have very different spectra than the resulting fields. The initial error fields were designed to have horizontal spectra with very low energy in the synoptic scales and greater energy in the subsynoptic scales (see VE for description of initial error spectra).

4) The horizontal error fields after about 24 h of integration consist of the local eddy-trainlike synoptic-scale structures associated with the upper-level trough and the surface low pressure. This is illustrated in Fig. 1 where the 500-mb MM4 forecast superimposed on the sea-level pressure field is displayed with the corresponding 500-mb geopotential error field for the LECY, LLJE, and EXCY cases.

b. Linear tangent integrations

The linear tangent numerical model described in section 2 was integrated for each synoptic case starting at the t_1 nonlinear integration time. The t_1 time was chosen to be equal to or larger than the model spinup time, which is typically 12–24 h.

The t_1 time was 24 h for the LECY and LLJE experiments and 12 h for the EXCY experiment. The initial fields for the linear model were, therefore, the t_1 time error fields based on the nonlinear experiments. Similarly, the nonlinear forecast fields were used as the basic-state fields for the linear model integrations. These basic-state data consisted of the discrete time series of nonlinear forecast data associated with the $t_n = t_1 + n\Delta t$ nonlinear forecast times, where Δt was 6 h. The basic-state fields, therefore, were updated abruptly every 6 h throughout linear integration.

The 24-h linear tangent solutions ($t = t_1 + 24$ h) displayed in Fig. 2 are very similar to the nonlinear integration error fields shown in Fig. 1. The pattern similarity between the linear and nonlinear solutions is greater than the similarity in amplitudes, especially for the LECY and LLEY cases (Figs. 2a,b). The error amplitudes are larger for the linear tangent solutions than for the nonlinear integrations. In the EXCY linear solution (Fig. 2c) the eddylike pattern along the east coast of the United States is lagged relative to the nonlinear case in the direction marked by the thick line in Fig. 2c. This is probably a consequence of the southwest–northeast fast propagation of the synoptic system in the EXCY forecast, which was not adequately represented by the 6-h interval in the basic-state time series used for the tangent linear integrations. We have performed an additional tangent linear integration updating the basic state every 3 h. This has somewhat improved the linear solution for the EXCY case (Fig. 3).

These results undoubtedly show that the initial error evolution is well represented by the tangent linear solutions for the forecast model used in this study. We believe that this conclusion would apply to other models and other synoptic cases providing the spatial and temporal scales are similar to the cases used in this study.

Lacarra and Talagrand (1989) have shown that the evolution of dominant components of the forecast errors in their shallow-water f-plane model could be approximated by the solutions of the tangent model based on the time-independent coefficients. It is important to test this possibility for the realistic forecast model because the initial error evolution estimates for the operationally used prognostic models can be based only on the initial basic states. In the next section we further simplify our linear tangent model by assuming a time-independent basic state. For brevity this version of the linear model is hereafter referred to as the constant tangent model.

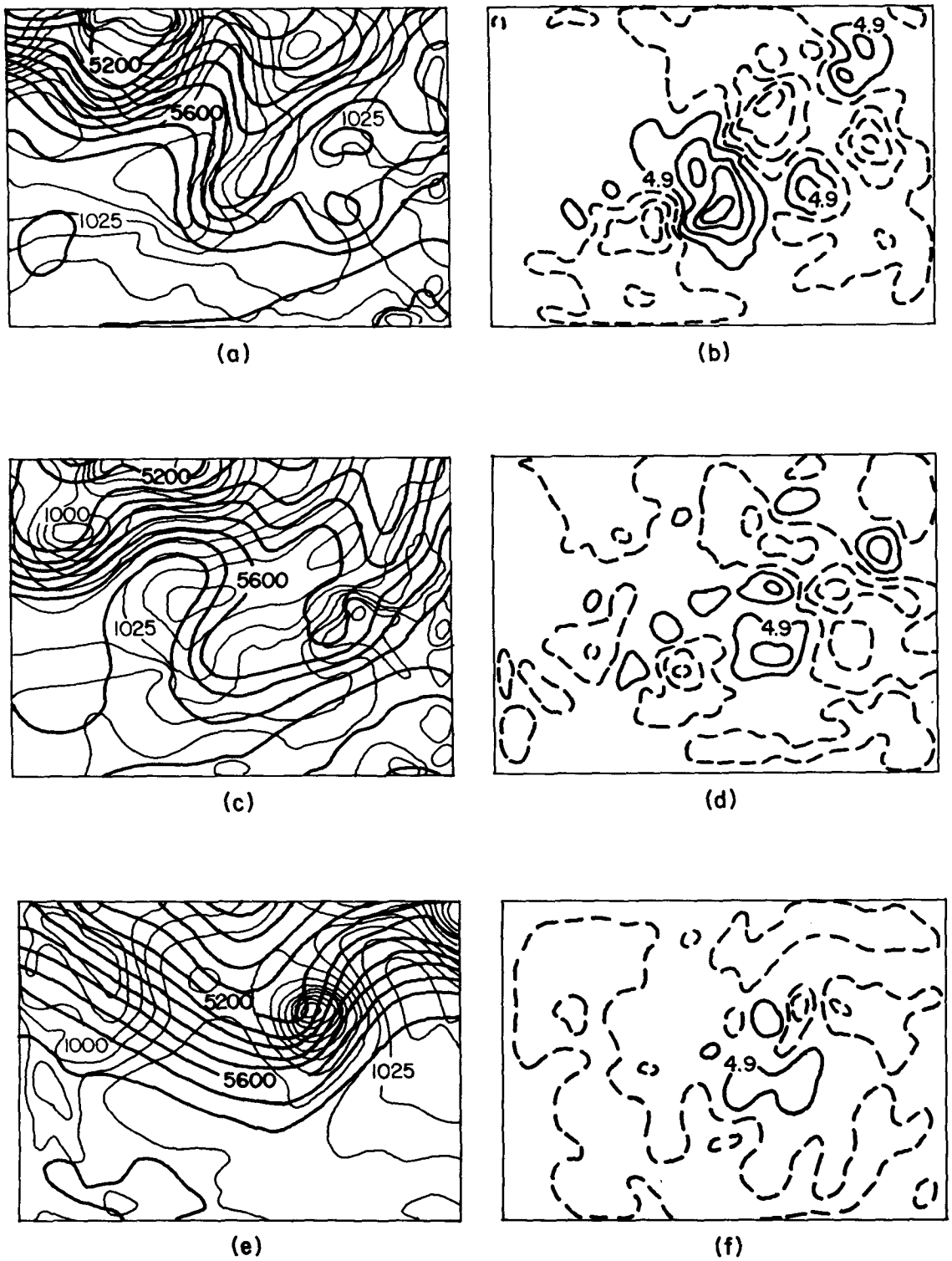

FIG. 1. 500-mb geopotential forecast superimposed upon sea-level pressure forecast for the LECY, LLJE, and EXCY cases, panels (a), (c), and (d), respectively. Corresponding 500-mb geopotential error fields are shown in panels (b), (d), and (f), respectively (contour interval is 5 m).

c. Constant tangent model

The experiment design, using the constant tangent model, was the same as for the experiments described in section 3b, only the basic-state data associated with the t_1 nonlinear forecast time were applied throughout the linear integration. Additionally, basic-state winds were modified by subtracting the three-dimensional domain-averaged wind. This was performed because the domain-averaged time-dependent wind was weaker than the domain-averaged wind in the initial basic state for some synoptic cases. The otherwise large winds caused too rapid advection of the perturbations out of the domain of integration. The modification of the basic-state wind by subtracting the constant value is equivalent to performing the integrations in a frame of reference moving at a spatially and temporally constant speed. This kind of coordinate transformation changes only the oscillatory portion of the linear solution. For example, this is equivalent to a spatially constant phase shift for the standard linear stability models based on the zonally uniform basic states.

FIG. 3. As in Fig. 2c, but for the experiment with the basic state changing every 3 h.

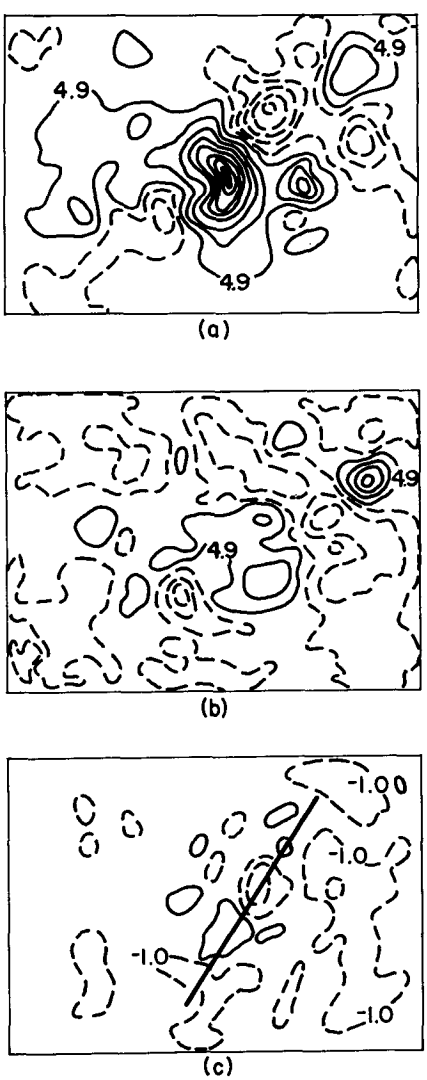

FIG. 2. 24-h tangent linear model 500-mb geopotential perturbation solution for the LECY, LLJE, and EXCY cases. Contour interval is 5 m.

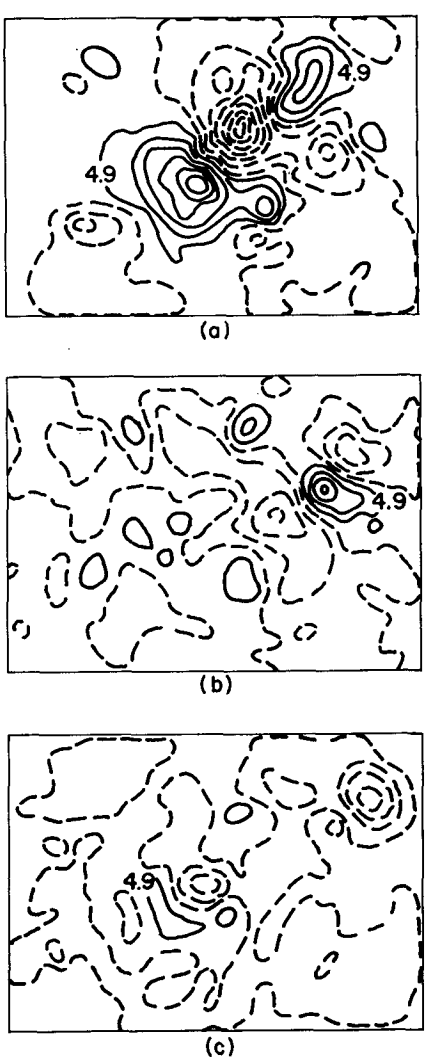

FIG. 4. As in Fig. 2, but for the constant tangent model experiment.

The constant tangent model solutions displayed in Fig. 4 are similar to the solutions based on the nonlinear model integrations (Fig. 1), but are less similar than the tangent model solutions based on the time varying basic states (Fig. 2). The fields displayed in Fig. 4 appear phase shifted with respect to the fields shown in Fig. 1 and Fig. 2. This conclusion especially applies to the LECY and LLJE cases. For example, the double-dipole pattern shown in Fig. 4a is lagged toward the southwest corner of the domain with respect to the pattern shown in Fig. 1a. To the extent that similarity between compared fields is based on gross features and

pendent basic state approximation can be extended up to 36 h of integration ($t_1 + 36$) for the LECY and LLJE cases (not shown).

The constant tangent model results are less conclusive for the EXCY case [see the (c) panels in Figs. 1, 2, and 4] because the error magnitudes are smaller overall and are not organized in coherent structures as much as for the LECY and LLJE cases.

The results presented in this section indicate that a linear model can be used for studying initial error evolution for the primitive-equation mesoscale model. In the next section we discuss this application of the linear MM4.

4. Unstable linear solutions

An interesting question associated with the results described in the previous section pertains to the reason why the nonlinear and tangent linear integrations show initial error decay for dynamically unstable synoptic development such as the EXCY case. In this section we use simple method based on the linear theory to study this question. We also discuss the application of the linear theory to general initial error estimate problems using the mesoscale linear model.

a. Linear theory

The linear model represented by (1a)–(1g) can be written as:

$$\frac{\partial V}{\partial t} = \mathbf{L}[\mathbf{V}(x, y, \sigma, t)] \qquad (2)$$

where $\mathbf{V}$ is the model solution vector and $\mathbf{L}$ is the linear operator. When the right-hand side of (2) is written in the finite difference form, the operator $\mathbf{L}$ is a matrix.

Similar to other studies based on linear models (e.g., Branstator 1985; Farrel 1988), we express the vector $\mathbf{V}$ in terms of the matrix $\mathbf{L}$ eigenvectors

$$\mathbf{V} = \sum_j a_j(t) v_j(x, y, \sigma) \qquad (3)$$

where a_j is the projection coefficient associated with the eigenvector v_j. The solution of (2) is easily evaluated using (3) and the biorthogonal property of the adjoint eigenvectors associated with the matrix $\mathbf{L}$ (e.g., Branstator 1985). The inner product of (2) with the jth adjoint eigenvector renders the solution for the coefficient $a_j(t)$. The total solution for $\mathbf{V}$ would then be the sum of all normal modes $a_j(t)v_j(x, y, \sigma)$:

$$\mathbf{V} = \sum_j a_j(0) e^{i\lambda_j t} v_j(x, y, \sigma) \qquad (4)$$

where λ_j's are the eigenvalues of matrix $\mathbf{L}$, $a_j(0)$'s are the initial projection coefficients associated with the eigenvectors v_j's, and $i = \sqrt{-1}$. In general, the λ_j's have complex values. The normal modes in (4) are, therefore, decaying, oscillatory, or growing depending on the value of λ_j. In order to determine these solutions the eigenvalue/eigenvector analysis for the matrix $\mathbf{L}$ should be performed.

Two limitations are readily considered for using this approach: 1) computation of the matrix $\mathbf{L}$ entries may be very costly because one time step integration of the linear model is required for each column of $\mathbf{L}$, and 2) the eigenvalue/eigenvector evaluation for the large size matrix may be beyond a practical computational limit. The model matrix for the numerical experiments discussed in the previous section has $(125\ 550)^2$ entries. Clearly, direct eigenvalue/eigenvector analysis is virtually impossible for this size matrix. In order not to modify our experiment design by either using a smaller integration domain size or larger grid interval, both of which alter the solutions considerably, we simplify our approach by considering the following conditions: 1) we are interested only in the unstable solutions of the linear system (2), and 2) evaluation of a single unstable linear solution is sufficient for our present purpose of estimating:

(i) the dependence of nonlinear results on the specific choice of the initial perturbation and the evolution of linear unstable perturbation in the nonlinear environment;

(ii) spatial scales of the linear unstable solution for different basic states and how they relate to the nonlinear initial error fields; and

(iii) temporal variation of basic state stability.

A suitable method for treating this simplified problem is the "power method." This method is based on temporal asymptotic behavior of the linear model solutions. The long-time solution of the system (2) would be dominated by the most unstable normal mode. Therefore, the long-time integration of our constant tangent linear numerical model would converge toward the most unstable linear normal mode associated with the given basic state.

We should point out that the most unstable normal mode is not necessarily the most unstable short-time perturbation associated with the given basic state (e.g., Farrell 1988; Lacarra and Talagrand 1988; Valdes and Hoskins 1988). This is because the eigenvectors of the model matrix $\mathbf{L}$ are not typically orthogonal to each

other, which enables superposition of several normal modes to grow faster than the most unstable normal mode for a short time. The linear theory shows that the linearly optimal, most unstable, initial perturbations can be determined by performing the eigenanalysis of the "amplification matrix" such as discussed in Lacarra and Talagrand's (1989) study. However, it is unclear yet what is the best way to apply this approach to the complete, primitive equation model. This is because it is unclear what is the best integral measure of the perturbation amplitude (norm) for the primitive equation system. The method discussed in the Lacarra and Talagrand's study depends crucially on this measure because this method is based on the adjoint linear operator, which is defined with respect to selected norm. Consequently, the results and conclusions based on this method can be very sensitive to the properties of selected integral perturbation amplitude measure. We believe that this sensitivity should be tested carefully. More research is needed in this area and we are currently developing the adjoint of the LMM4 in order to study this problem. In the present study we take simple approach of evaluating a single unstable linear model solution.

b. The most unstable normal mode

The 12-day integrations with the constant tangent linear model were performed for the LECY, LLJE, and EXCY cases using the t_1 time nonlinear forecast fields as the basic state data.

Perturbation fields similar to the nonlinear error fields were used as the initial data for the long-time constant tangent model integrations. Several different initial conditions were tested for each basic state. The long-time solutions, hereafter referred to as asymptotic solutions, originating from these slightly different initial conditions have converged toward the same spatial structure with slightly different magnitudes. Since the magnitudes of the linear model solutions are arbitrary, we present the numerical results of only one asymptotic solution for each basic state.

We would like to point out that the integration period of 12 days may not be long enough to yield the pure, most unstable, normal mode solution for any arbitrarily chosen basic state since the single most unstable mode may still not dominate all other modes by this time. However, the small differences between successive solutions after one week of integration in our experiments indicate that the 12-day solution is close to the most unstable perturbation associated with the studied basic states. Accordingly, we refer to the 12-day constant tangent model solution as the "most unstable normal mode."

Figure 5 shows the "most unstable normal mode" for the 500-mb geopotential height field for the LECY, LLJE, and EXCY cases. These fields resemble the short-time nonlinear or tangent linear solutions (corresponding panels in Figs. 1, 2, and 3), in terms of spatial scales, location of the maximum magnitudes, and orientation of the main peturbation "eddy-train" relative to the basic-state flow, but many details are different with respect to the nonlinear results. The differences between the most unstable asymptotic solution and the short-time error fields are largest for the EXCY case because the nonlinear and tangent linear solutions for this case are decaying, unlike the unstable asymptotic constant tangent model solution. The vertical structure of the "most unstable normal mode" is also similar to the short-time nonlinear or tangent linear solutions, especially for the growing error cases (LECY and LLJE). For each case, the barotropic mode and gravest baroclinic vertical mode are dominant (Fig.

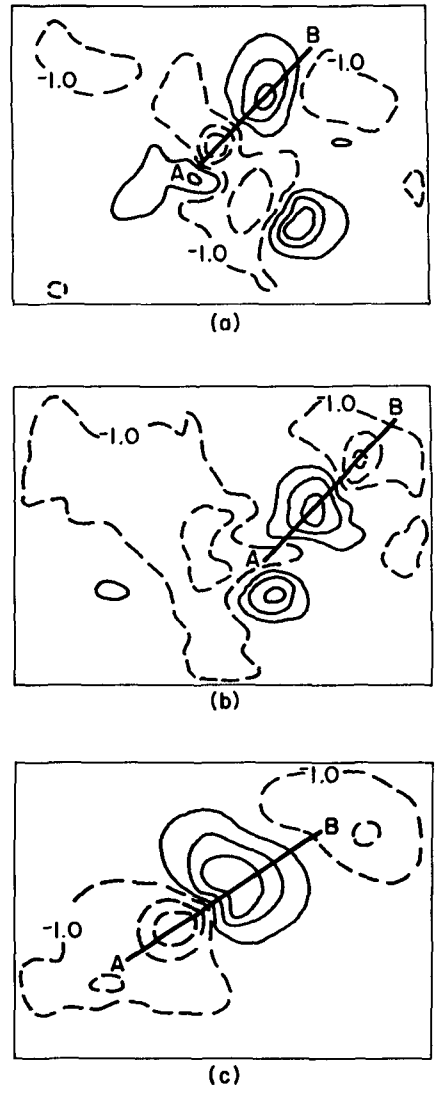

FIG. 5. 12-day constant tangent model 500-mb geopotential perturbation solution for the LECY, LLJE, and EXCY cases, panels (a), (b), and (c), respectively. Perturbation magnitudes are scaled by 1000.

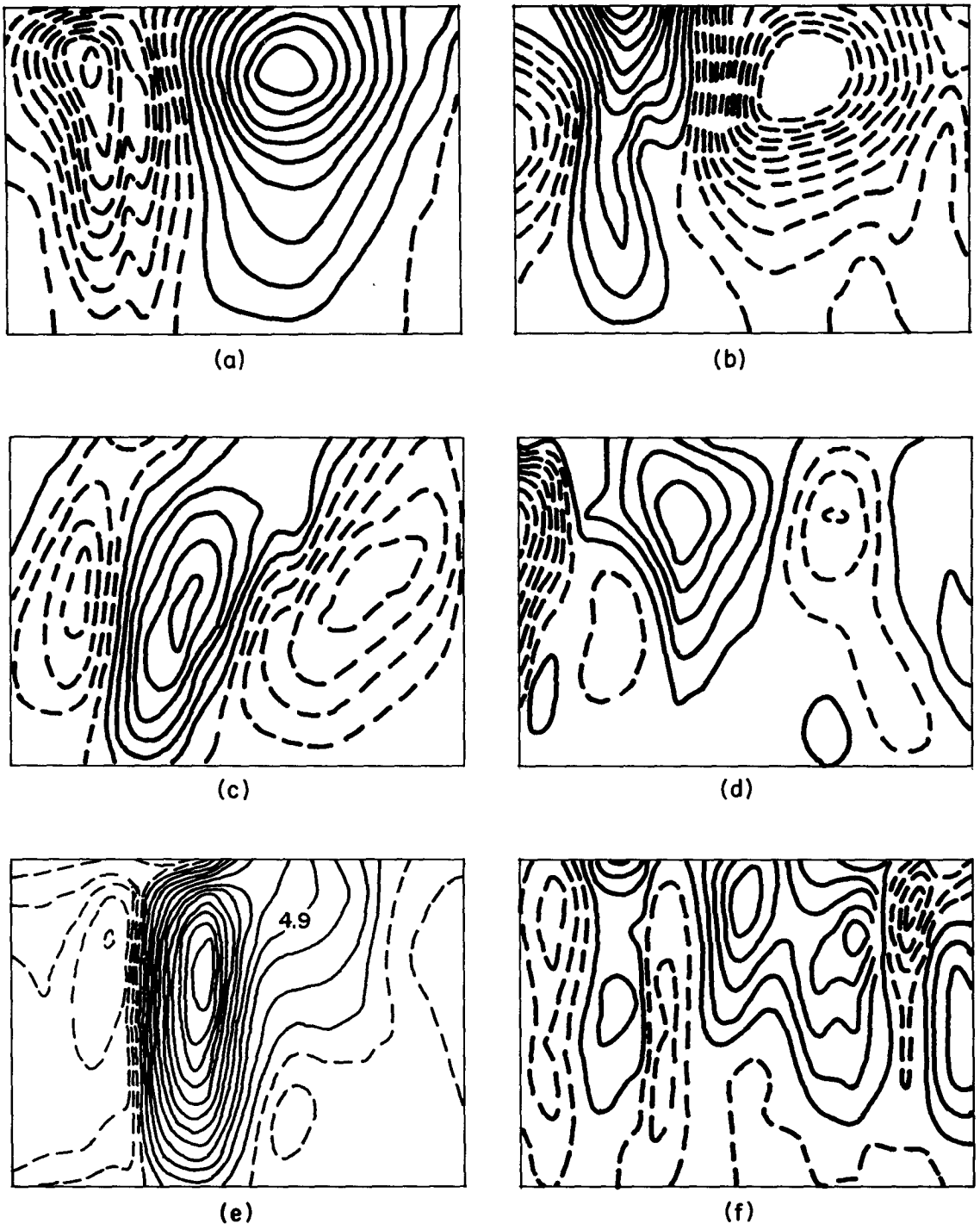

FIG. 6. Vertical cross section of geopotential perturbations along A–B segments demarked in Fig. 5. Panels (a), (c), and (e) represent 12-day constant tangent model solutions and panels (b), (d), and (f) represent nonlinear forecast errors for the forecast times shown in Fig. 1.

6). However, similar to the horizontal fields, differences in details are large (compare panels (a), (c), and (e) with (b), (d), and (f), respectively, in Fig. 6).

The "most unstable normal mode" *e*-folding time is estimated using the last 24 h of long-time constant tangent model integrations. The eigenvalue associated with the "most unstable normal mode" was computed using:

$$\lambda^* = \frac{1}{2\Delta t} \ln\alpha$$

where α is given by

$$\alpha = \frac{1}{N} \sum_{k=1}^{N} \alpha_k \quad \text{and}$$

$$\alpha_k = \frac{\int_D \mathbf{V}^2(x, y, \sigma, t_k + \Delta t) dD}{\int_D \mathbf{V}^2(x, y, \sigma, t_k) dD}, \qquad (5)$$

D is the three-dimensional model domain, $N = 24/\Delta t$, and $\mathbf{V}$ is the linear model solution vector as before. The e-folding time is given by $t_e = 1/\lambda^*$.

The e-folding times for the LECY, LLJE, and EXCY cases are, respectively, 36, 69, and 24 h. These results suggest largest asymptotic instability associated with the EXCY case, weaker instability for the LECY case, and weak instability associated with the LLJE case. On the other hand, the nonlinear and tangent linear results show largest rms perturbation growth for the LECY case, weak growth for the LLJE case, and decay for the EXCY case. Possible explanation for this discrepancy associated with the EXCY case was investigated by performing the following experiments.

First, the "most unstable normal mode" associated with the $t_1 = 12$ h EXCY nonlinear forecast was used as the initial perturbation for a nonlinear 1-day integration (12 h + 24 h). We have arbitrarily chosen small magnitudes for this initial perturbation. For example, the rms magnitude for the 500-mb geopotential field was about 0.6 m. The rms magnitudes of the nonlinear model errors originating from this initial perturbation grow for the first 6 h of integration and then level off for the remaining 18 h. The initial perturbation in this experiment is advected rapidly toward the NE along the explosive cyclone track. The structure of this perturbation is also changed from the initial three-element eddylike pattern (Fig. 5c) to a dipole eddylike pattern at the end of integration period (not shown).

These results show that the linear unstable perturbation is also unstable with respect to the nonlinear flow for a limited period of time, as expected. These results also indicate that the initial perturbation used for the nonlinear experiment described in section 3a was not appropriate for estimating sensitivity of the EXCY forecast to initial errors. Consequently, the results of this nonlinear experiment were misleading.

The evolution of the "most unstable normal mode" initial perturbation in the present nonlinear experiment shows that the nonlinearity and rapid change of the flow can significantly alter the initial perturbation evolution with respect to the linear model prediction after a relatively short period of time. This conclusion agrees with the tangent linear model results for the EXCY case presented in section 3b. These results show that the solution based on the basic state with the update interval of 3 h is slightly better than the solution based on the basic state with the update interval of 6 h.

In the second experiment, the constant tangent model long-time integration is performed using the $t_1 = 36$ h nonlinear forecast fields as the basic state data instead of the $t_1 = 12$ h fields used in the previous experiment. The e-folding time for the "most unstable normal mode" associated with this basic state is about 36 h, which is 12 h longer than the e-folding time associated with the $t_1 = 12$ h basic state. This result suggests increasing stability associated with the EXCY time evolution, which may also be considered as an influencing factor upon the error decay associated with the second half of the forecast period for the EXCY case.

5. Summary and conclusions

The hypothesis that the short-time evolution of forecast errors originating from initial data uncertainties can be approximated by linear model solutions was studied using a linear version of a complex limited-area model. The linearization was performed with respect to a temporally and spatially varying basic state produced by the complete nonlinear model real data forecast.

The short-time tangent linear model solutions and the error fields based on the nonlinear integrations are virtually identical in shape and slightly different in amplitudes. These results demonstrate that the major portion of the initial forecast errors can be described by the tangent model solutions for the complete mesoscale forecast model for periods of 1–1.5 days duration.

Similar to Lacarra and Talagrand's (1989) results, our experiments suggest that the linear model solutions based on time-independent basic states are also good approximations of the initial error evolutions, providing the forecast fields are not changing rapidly in time.

These results suggest that linear theory can be used for the initial error evolution studies for the realistic prognostic models. In this study we have shown one such application of the linear limited-area model using a rather simple, but easily implemented method. The asymptotic most unstable linear model solutions are evaluated for several complex basic states. These solutions are then used to show that the initialization of the nonlinear model with the linear unstable solution superimposed on the initial basic fields can produce a very different error evolution than the initialization based on an arbitrarily chosen perturbation field. For example, for the explosive cyclogenesis case, the forecast errors based on the linear unstable initial perturbation grow unlike the errors originating from the arbitrarily selected initial perturbation. The nonlinear integrations based on the asymptotically most unstable linear initial perturbation also indicate that rapid change of the basic flow and nonlinearity can produce

large deviations from the linear model predicted error evolution for the same unstable initial perturbation for periods longer than some critical finite time. This critical time depends on the time evolution of the given synoptic case.

The horizontal and vertical scales of the asymptotic most unstable linear solutions and the 24-h nonlinear error fields are very similar. This result additionally suggests that the evaluation of the unstable linear solutions associated with the initial basic state can be used for short-to-medium term forecast skill estimates.

The linear theory and recent studies based on simplified dynamical models clearly show that the best estimate of the most unstable initial perturbations is provided by the nonexponential (finite-time), most unstable linear perturbations. To the authors' knowledge, the extension of the methods used for the simplified dynamical models for studying this problem is not trivial for the complex primitive-equation model. This is caused by the difficulty in defining the best error norm for the primitive system. We are currently developing the adjoint of the linear MM4 in order to study this problem.

Acknowledgments. The author would like to thank Ronald Errico, Grant Branstator, Joe Tribbia, and Ying-Hwa Kuo for fruitful discussions regarding this work.

REFERENCES

Anthes, R. A., E. Y. Hsie and Y. H. Kuo, 1987: Description of the Penn State/NCAR Mesoscale Model Version 4 (MM4). NCAR Tech. Note NCAR/TN 282 + STR, 66 pp. [Available from the National Center for Atmospheric Research, P.O. Box 3000, Boulder, CO 80307.]

Branstator, G., 1985: Analysis of general circulation model sea surface temperature anomaly simulations using a linear model. Part II: Eigen analysis. *J. Atmos. Sci.*, **42,** 2242–2254.

Farrel, B., 1988: Optimal excitation of neutral Rossby waves. *J. Atmos. Sci.*, **45,** 163–172.

Kallen, E., and X. Y. Huang, 1988: The influence of isolated observations on short-range numerical weather forecast. *Tellus,* **40A,** 324–336.

Kuo, Y.-H., and S. Low-Nam, 1990: Prediction of nine explosive cyclones over the western Atlantic Ocean with a regional model. *Mon. Wea. Rev.*, **118,** 3–25.

Lacarra, J.-F., and O. Talagrand, 1989: Short-range evolution of small perturbations in a barotropic model. *Tellus,* **40A,** 81–95.

Lorenz, E. N., 1969: The predictability of flow which possesses many scales of motion. *Tellus,* **21,** 289–302.

Thompson, P. D., 1957: Initial state as a factor in the predictability of large scale atmospheric flow patterns. *Tellus,* **9,** 275–295.

Valdes, P. J., and B. J. Hoskins, 1988: Baroclinic instability of the zonally averaged flow with boundary layer damping. *J. Atmos. Sci.*, **45,** 1584–1593.

Vukicevic, T., and J. Paegle, 1989: The influence of one-way interacting lateral boundary conditions upon predictability of flow in bounded numerical models. *Mon. Wea. Rev.*, **117,** 340–350.

——, and R. M. Errico, 1990: The influence of artificial and physical factors upon predictability estimates using a complex limited-area model. *Mon. Wea. Rev.*, **118,** 1460–1482.